Neurobiology of Disease

Presenilin and APP Regulate Synaptic Kainate Receptors

Gaël Barthet,* Ana Moreira-de-Sá,* Pei Zhang, Séverine Deforges, Jorge Castanheira, Adam Gorlewicz, and Christophe Mulle

Université of Bordeaux, CNRS, Interdisciplinary Institute for Neuroscience (IINS), UMR 5297, F-33000 Bordeaux, France

Kainate receptors (KARs) form a family of ionotropic glutamate receptors that regulate the activity of neuronal networks by both presynaptic and postsynaptic mechanisms. Their implication in pathologies is well documented for epilepsy. The higher prevalence of epileptic symptoms in Alzheimer's disease (AD) patients questions the role of KARs in AD. Here we investigated whether the synaptic expression and function of KARs was impaired in mouse models of AD. We addressed this question by immunostaining and electrophysiology at synapses between mossy fibers and CA3 pyramidal cells, in which KARs are abundant and play a prominent physiological role. We observed a decrease of the immunostaining for GluK2 in the stratum lucidum in CA3, and of the amplitude and decay time of synaptic currents mediated by GluK2-containing KARs in an amyloid mouse model (APP/PS1) of AD. Interestingly, a similar phenotype was observed in CA3 pyramidal cells in male and female mice with a genetic deletion of either presenilin or APP/APLP2 as well as in organotypic cultures treated with γ-secretase inhibitors. Finally, the GluK2 protein interacts with full-length and C-terminal fragments of APP. Overall, our data suggest that APP stabilizes KARs at synapses, possibly through a transsynaptic mechanism, and this interaction is under the control the γ-secretase proteolytic activity of presenilin.

Key words: **Alzheimer's disease; APP; kainate receptors; presenilin; synapse**

Significance Statement

Synaptic impairment correlates strongly with cognitive deficits in Alzheimer's disease (AD). In this context, many studies have addressed the dysregulation of AMPA and NMDA ionotropic glutamate receptors. Kainate receptors (KARs), which form the third family of iGluRs, represent an underestimated actor in the regulation of neuronal circuits and have not yet been examined in the context of AD. Here we provide evidence that synaptic KARs are markedly impaired in a mouse model of AD. Additional experiments indicate that the γ-secretase activity of presenilin acting on the amyloid precursor protein controls synaptic expression of KAR. This study clearly indicates that KARs should be taken into consideration whenever addressing synaptic dysfunction and related cognitive deficits in the context of AD.

Introduction

Kainate receptors (KARs) form a family of ionotropic glutamate receptors related to, but distinct from, AMPA (AMPARs) and NMDA receptors (NMDARs), which are composed of the tetrameric assembly of subunits (GluK1–GluK5) encoded by five genes (*grik1–grik5*; Contractor et al., 2011; Lerma and Marques, 2013). KARs regulate the activity of neuronal networks by acting at presynaptic and postsynaptic levels, through either an ionotropic or a metabotropic action (Mulle and Crépel, 2021). KARs are abundantly expressed in the brain, in which heteromeric GluK2/GluK5 KARs appear to be a major isoform (Wenthold et al., 1994). The physiological role of KARs has been extensively studied at hippocampal mossy fiber (Mf) synapses between the dentate gyrus granule cells and CA3 pyramidal cells (Carta et al., 2014b). KARs act at a presynaptic level to regulate short-term and long-term synaptic plasticity and spike transfer (Contractor et al., 2001; Sachidhanandam et al., 2009). In addition, postsynaptic KARs comprising the GluK2 subunit also mediate slowly decaying EPSCs of small amplitude (Castillo et al., 1997; Mulle et al., 1998), which appear to be important for the temporal integration of signals during high-frequency bursts of synaptic input (Pinheiro et al., 2013). In CA3 pyramidal cells, KARs show a highly segregated subcellular distribution, being concentrated at Mf–CA3 synapses and excluded from other synaptic compartments or extracellular domains (Castillo et al., 1997; Fièvre et al., 2016). This strict

Received Feb. 10, 2022; revised Aug. 25, 2022; accepted Sep. 27, 2022.

Author contributions: G.B. and C.M. designed research; G.B., A.M.-d.-S., P.Z., S.D., J.C., and A.G. performed research; G.B., A.M.-d.-S., and P.Z. analyzed data; C.M. wrote the paper.

This work was supported by the Centre National de la Recherche Scientifique (CNRS); a French ANR (Agence Nationale de la Recherche) PREPLASH Project grant; a grant from the Fondation France Alzheimer; and the Erasmus Mundus program "European Neuroscience Campus" from the Seventh Framework Programme (to P.Z.). We thank Justine Gautron for her help with some biochemistry experiments. We also thank the Bordeaux Imaging Center (BIC), a service unit of the CNRS-Institut National de la Santé et de la Recherche Médicale and Bordeaux University, which is a member of the national infrastructure France BioImaging, for help in performing microscopy.

*G.B. and A.M.-d.-S. contributed equally to this work.

The authors declare no competing financial interests.

Correspondence should be addressed to Christophe Mulle at christophe.mulle@u-bordeaux.fr.

https://doi.org/10.1523/JNEUROSCI.0297-22.2022

compartmentalization relies on multiple mechanisms, including a stringent control of the amount of GluK2 subunit. In CA3 pyramidal cells, the recruitment/stabilization of KARs by N-cadherins (Fièvre et al., 2016) and the transsynaptic complex formed by C1ql2/3 and neurexin, which binds to GluK2 and GluK4 subunits (Matsuda et al., 2016). In addition, Neto1 is an auxiliary subunit of native KARs, which determines key properties of KARs, such as their high affinity for agonist and slow kinetics, and contributes to synaptic KARs at Mf–CA3 synapses (Straub et al., 2011; Tang et al., 2011; Copits and Swanson, 2012). KARs have been implicated in several neurologic and psychiatric disorders in genetic linkage studies, although much remains to be explored for most of the diseases (Lerma and Marques, 2013). A strong link, however, exists between KARs and the clinically relevant chronic phase of temporal lobe epilepsy (TLE; Crépel and Mulle, 2015). Pathophysiological mechanisms involve KARs composed of GluK2/GluK5, which are ectopically expressed at recurrent Mf synapses onto dentate gyrus cells (Epsztein et al., 2005); these aberrant KARs participate in the generation of recurrent seizures in models of chronic epilepsy (Peret et al., 2014). Although epilepsy is frequently associated with Alzheimer's disease (AD; Vossel et al., 2017), there is currently no report on how KAR function may be affected in the context of AD.

Mutations of two presenilin (PS) paralogs PS1 or PS2 are causal to familial forms of AD (FAD; Sherrington et al., 1995). PS is the catalytic subunit of the intramembrane protease γ-secretase, which cleaves several type 1 transmembrane proteins (De Strooper et al., 1998). Substrates of γ-secretase are mostly membrane-bound polypeptides derived from the shedding of the extracellular domain of transmembrane proteins usually by members of the ADAM (A Disintegrin And Metalloproteinase) family of metalloproteinases (Barthet et al., 2012). PS is particularly known to be involved in the processing of the amyloid precursor protein (APP), producing the Aβ peptides and the APP-intracellular domain. The γ-secretase complex also promotes the cleavage of a large number of cell surface proteins found at synaptic contacts, such as transsynaptic adhesion molecules including cadherins, ephrin ligands, and receptor EphB (Barthet et al., 2011). PS has been reported to regulate synaptic transmission at a presynaptic site (Barthet et al., 2018). The prevalence of an epileptic-like phenomenon in AD and the role of KAR in epilepsy made us investigate a possible regulation of KARs in the context of AD. We combined immunostaining and electrophysiology to investigate the effect of PS and APP processing on KAR function and synaptic expression. By comparing three mouse models, an amyloid mouse model expressing a FAD form of PS1 (ΔE9), and conditional knock-out (KO) model of PS and APP/APLP2, we identified APP and its processing by PS as strong regulators of synaptic KARs.

Materials and Methods

Mice. The APP/PS1 mice used (Jankowsky et al., 2004; Garcia-Alloza et al., 2006) were obtained from The Jackson Laboratory and used according to regulations of the University of Bordeaux/Centre National de la Recherche Scientifique (CNRS) Animal Care and Use Committee. The PS1fl/PS2KO mice were produced by mating PS1floxed mice (catalog #007605) with PS2-KO mice (#005617) lines from The Jackson Laboratory (Barthet et al., 2018). The APP/APLP2 double-floxed mice were produced by crossing APP floxed with APLP2 floxed homozygotic mice lines obtained from Ulrike Müller (University of Heidelberg, Heidelberg, Germany). Throughout their lives, all mice were group housed, ranging from 4 to 10 animals per cage. Food and water were provided *ad libitum*. The transparent Plexiglas cages (38.1 × 19.1 × 12.7 cm) were maintained on a 12 h dark/light cycle, kept in a temperature-regulated room, and protected from exterior pathogens by a filter. Experiments on APP/PS1 mice were performed in the light phase of the circadian cycle in 6-month-old (26–32 weeks) mice and age-matched wild-type (WT) littermates. Experiments on PS1fl/PS2KO and APP/APLP2 KO were performed on postnatal day 40 (P40) to P60 mice, 3 weeks after viral manipulation.

Viral gene transfer and stereotaxic delivery. Mice (age, P22–P30) were anesthetized by isoflurane inhalation and injected with buprenorphine to prevent postsurgery pain. Four hundred nanoliters of AAV (adeno-associated virus) solution at 5.10E11 (1×10^{E5} particles) was injected using a micropump and syringe (NanoFil, WPI) at the rate of 75 nl/min in the dentate gyrus (DG; *y*, 2.2 mm from λ; *x*, $\pm$ 2.5 mm from sagittal suture; *z*, −2.35 mm from the skull) to infect CA3 neurons. The spreading of viruses allowed the infection of a large part of the hippocampus (radius, ~1 mm) to produce numerous slices for immunohistochemistry or electrophysiology. Experiments were performed at least 3 weeks postinjection.

Slice preparation. The anesthesia drug (ketamine, 75 mg/kg; xylazine, 10 mg/kg) was diluted in saline and injected intraperitoneally into the mouse 5 min before decapitation or transcardial perfusion followed by decapitation. The head was immediately placed into a Petri dish filled with iced artificial CSF (aCSF) mixed with a blender, as follows: 120 mM NaCl, 26 mM $NaHCO_3$, 2.5 mM KCl, 1.25 mM NaH_2PO_4, 2 mM $CaCl_2$, 1 mM $MgCl_2$, 16.5 mM glucose, 2.8 mM pyruvic acid, and 0.5 mM ascorbic acid, at pH 7.4 adjusted by saturating with carbogen (95% O_2 and 5% CO_2), and an osmolarity of 305 mOsm. Parasagittal slices (300 µm) were cut from brain hemispheres using a vibratome (model VT1200S, Leica Microsystems). Slices were then transferred to aCSF for 20 min at 33°C and thereafter maintained at room temperature until required.

Slice culture preparation and treatment. Organotypic hippocampal slices (300 µm thickness) were prepared from P5 to P7 WT C57BL/6J mice according to the guidelines of the University of Bordeaux/CNRS Animal Care and Use Committee. Three to 4 d after plating, the medium was replaced and then changed every 2–3 d. After 10 d *in vitro* (DIV), the γ-secretase inhibitor (GSI) L685,458 was added at 10 μM. After a period of 4–6 d of treatment, organotypic slices were used for electrophysiology experiments.

Electrophysiological recordings. The recording chamber of the electrophysiology setup was perfused with oxygenated aCSF. CA3 pyramidal neurons in the CA3b subregion were identified by differential interference contrast microscopy using a fixed-stage upright microscope (model BX51WI, Olympus) equipped with a 60× magnification immersion objective at room temperature, and whole-cell patch-clamp configuration was achieved with borosilicate glass capillaries with resistance values ranging from 3 to 5 MΩ. Voltage-clamp recordings were performed with an internal solution containing the following (in mM): 125 $CsCH_3SO_3$, 2 $MgCl_2$, 4 NaCl, 5 phosphocreatine, 4 Na_2ATP, 10 EGTA, and 10 HEPES, at pH 7.3 adjusted with CsOH, and an osmolarity of 300 mOsm. Bicuculline (10 μM) was added to the bath to inhibit $GABA_A$ receptors. Mf-CA3 EPSCs were evoked by electrical stimulation (200 µs, 10-20 µA) of the Mf tracts in the hilus of the dentate gyrus. Cells were allowed to stabilize for 5 min after the whole-cell configuration was established. To monitor the access resistance during the whole recording time, a hyperpolarizing voltage step (−5 mV, 10 ms) was applied at the beginning of each trace. Series access resistance was <20 MΩ, and when it changed by >30%, the recording was discarded. When held at −70 mV, neurons with a holding current >250 pA were also rejected. Mf synaptic currents were identified according to the following criteria: (1) large paired-pulse facilitation; (2) EPSCs with a steep rising phase (~1 ms); and (3) EPSCs that decay free of secondary peaks that might indicate the presence of polysynaptic contamination. Liquid junction potential correction was not used for measurements of membrane potentials. Unless stated differently, all baselines were established with a stimulation at 0.1 Hz and were compared with the same stimulation frequency after a drug application or stimulation protocol.

Recordings were made using an amplifier (model EPC10.0, HEKA Elektronik), filtered at 0.5–1 kHz and analyzed using IGOR

Pro and Neuromatic version 2.6 software. All drugs for electrophysiological experiments were obtained from Tocris Bioscience or Sigma-Aldrich, unless otherwise stated.

Immunostaining. Mice were initially anesthetized with a ketamine (75 mg/kg) and xylazine (10 mg/kg) solution diluted with saline solution, being injected intraperitoneally. When the animal was deeply unconscious, it was decapitated, and the brain was removed. The organ was immersed in isopentane (previously cooled with liquid nitrogen) to flash freeze the brain. Horizontal and cryosectioned slices (50 µm) were obtained using a cryostat (model CM3050S, Leica Microsystems) at −20°C. During brain slicing, slices were directly mounted on a SuperFrost Microscope (VWR), held at room temperature (RT) for a few minutes to obtain some humidity on mounted slices, then preserved at −80°C until immunostaining.

For immunohistochemistry of KAR subunits, the slices were initially fixed with Carnoy's solution (1:6 acid acetic/ethanol) for 20 min at RT, then was washed one time with PBS1X for 1 min at RT, after being permeabilized with Triton X-100 0.1% (for 30 min at RT). Before the incubation of primary antibodies, a blocking solution of Tween 0.05% plus newborn calf serum 5% was applied for 30 min at RT. Then sections were then incubated with primary antibodies. Rabbit polyclonal anti-GluK2 or anti-GluK5 antibodies (1:200) were used to label KAR subunits (catalog #180003 and #180103, respectively, Synaptic Systems) on APP/PS1 and CA3-PS-KO hippocampal sections, and a mouse polyclonal anti-GFP antibody (1:200) was used to label Cre-GFP to verify virus infection in CA3-PS-KO sections. This immunolabeling of GFP was necessary because the flash-freezing procedure damaged the 3D structure of GFP necessary to its intrinsic fluorescence. After performing three washes with PBS 1× (for 5 min at RT), a goat Alexa Fluor-647 anti-rabbit antibody (1:200) was used to detect the labeling on GluK2 or GluK5 subunits, whereas a donkey Alexa Fluor-488 anti-mouse antibody (1:200) was used to indicate the presence of Cre-GFP (2 h of incubation at RT). After performing three washes with PBS 1× (for 5 min at RT), the slices were mounted using DAPI-incorporated mounting media.

Coimmunoprecipitation and Western blotting. Neurons were grown in primary cultures for 2 weeks. Cells were scraped and lysed with the following lysis buffer: HEPES 50 mM, pH 7.35, NaCl 150 mM, glycerol 10%, dodecylmaltoside 0.5%, inhibitors of proteases, and phosphatases. After 2 h of rotation, the lysate was centrifuged for 15 min at 21,000 × *g*. The supernatant was used as a homogenate for Western blotting and as starting material for immunoprecipitation (IP). IP was performed using 10 µg of antibody/1 mg of neuronal lysates. Antibodies 22C11 (Millipore), 6E10 (BioLegend), and Y188 (Abcam) were used, respectively, against the Nter, the juxtamembrane region, and the Cter. Ig–protein complexes were pulled down by the addition of magnetic beads (SureBeads) and magnets. The samples were completed with Laemmli buffer. Proteins in the samples were separated by Western blotting using 4–20% gradient Tris-tricine gels. Membranes were probed for the proteins of interest, and chemiluminescent bands were detected with a CCD camera (ChemiDoc Imaging System, BIO-RAD).

Image acquisition. Slides were loaded into a slide scanner (model Nanozoomer 2.0HT, Hamamatsu), scanned at 20× magnification, and with a fixed additional lens at 1.75× magnification (resolution, 454 nm/pixel). Image acquisitions and settings were kept constant for all sections stained with a certain antibody. Additionally, to avoid biases in fluorescence intensity, all AD models and control cases were also scanned together. A γ correction of 1 was applied to all images to reach linearity in fluorescence signal, and images were then exported as tiff files using the NDP.view2 software (Hamamatsu) and analyzed using ImageJ Fiji (NIH).

Image analysis. ImageJ software was used to calculate raw pixel intensity of stratum lucidum of CA3 [region of interest (RO1)]. The data obtained with APP/PS1 and WT littermates were normalized to the mean raw intensity in WT. In the PS mouse model, acquisitions were performed in the stratum lucidum of CA3 [region of interest where genetic deletion occurs (RO1)] and in the CA1 cell layer [control region not affected by viral infection (RO2)]. The ratio of RO1/RO2 was calculated for each hippocampus to normalize the data obtained from immunostaining of PS-CA3-KO mice.

Experimental design and statistical analysis. Statistical analyses were performed with Prism9 (GraphPad Software). First, the normality of the dataset was tested using the D'Agostino–Pearson omnibus normality test. If data were normally distributed, a Student's *t* test, one-way ANOVA, or two-way ANOVA was performed; otherwise, nonparametric tests such as a Mann–Whitney test (for unpaired data) were used. For electrophysiological data, the *n* values can be found in the figure legends and correspond to the number of cells analyzed. Only one recording per slice was performed. Results are presented as the mean ± SEM, unless stated otherwise. Statistical differences were considered significant at $p < 0.05$. Identification of possible outliers and consequential removal was made by the Grubb's test (α set at 0.05 for outlier identification).

Results

Synaptic KARs are selectively downregulated at Mf–CA3 synapses in APP/PS1 mice

GluK2 containing KARs are highly enriched at hippocampal Mf–CA3 synapses (Carta et al., 2014b; Fièvre et al., 2016), as illustrated by the abundance of immunofluorescence signal in the stratum lucidum of wild-type mice, but not GluK2$^{-/-}$ mice (Fig. 1*A*,*B*). Using GluK2/3 and GluK5 selective antibodies (see Materials and Methods), we performed immunolabeling of hippocampal sections to compare KAR expression between WT and APP/PS1 mice. We detected a decrease in the immunofluorescence signal for GluK2 in the stratum lucidum of 6-month-old APP/PS1 mice compared with age-matched control mice (Fig. 1*C*,*D*). The quantification of mean pixel intensity within the stratum lucidum showed a significant decrease in GluK2 staining (Fig. 1*E*). However, although GluK2 combines with the GluK5 subunit to form native heteromeric KARs, we did not detect any significant change in the staining for the GluK5 subunit (Fig. 1*F*,*G*).

We have recently shown that the basal structural and functional properties, as well as presynaptic short-term plasticity at Mf–CA3 synapses are unaltered at 6 months in the APP/PS1 mouse model of AD (Viana da Silva et al., 2019). At this early stage, the APP/PS1 mice, however, display impairment in selected forms of synaptic plasticity, namely the lipid-based depolarization-induced potentiation of excitation (Carta et al., 2014a) and long-term potentiation of NMDA receptors (Viana da Silva et al., 2019). Using electrophysiological recordings in slices, we further tested whether synaptic KARs at Mf–CA3 synapses were impaired in 6-month-old APP/PS1 mice. We recorded from CA3 pyramidal cells in the whole-cell voltage-clamp mode, in the presence of the $GABA_A$ receptor blocker bicuculline (10 μM), to isolate glutamatergic inputs, and the selective NMDAR antagonist D-AP5 (50 μM), to block NMDAR-mediated currents. The peak amplitude of Mf–CA3 EPSCs evoked using minimal stimulation conditions with a glass electrode positioned close to the DG cell layer (Marchal and Mulle, 2004) at 0.1 Hz were not significantly different (Fig. 2*A*,*B*). As expected for Mf–CA3 synapses, the amplitude of evoked EPSCs markedly increased when the frequency of presynaptic stimulation was increased from 0.1 to 3 Hz (Fig. 2*A*,*C*). Although the absolute amplitude of Mf-EPSCs was quite variable at both frequencies of stimulation, we confirmed our previous report (Viana da Silva et al., 2019) that frequency facilitation was not different in WT versus APP/PS1 mice (Fig. 2*C*; WT, 5.47; vs APP/PS1, 5.02). We then applied GYKI-53784 at 25 μM in the bath to selectively block AMPARs, and thus isolate KAR-mediated EPSCs. KAR-EPSCs represent only a small fraction of the total

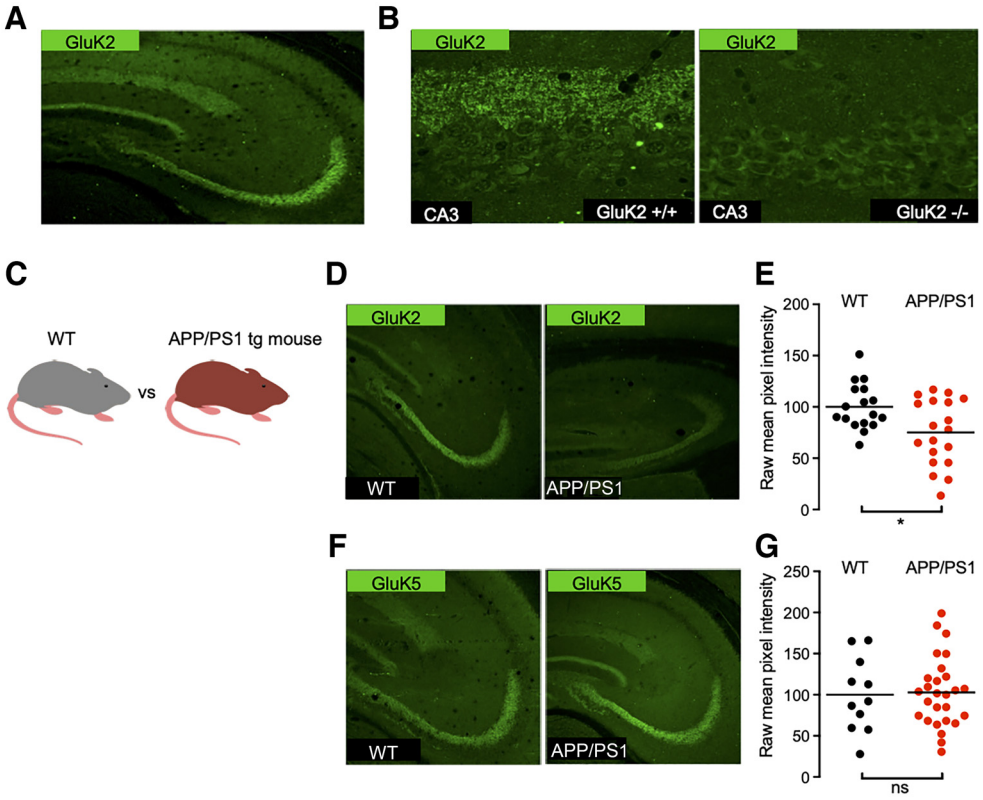

Figure 1. Distribution of kainate receptor subunits GluK2 and GluK5 in the hippocampus of WT and APP/PS1 mice. ***A***, Immunolabeling of mouse hippocampal sections reveals strong expression of GluK2 subunit in the stratum lucidum. ***B***, Zoom-in acquisitions on the CA3 area show staining adjacent to the CA3 pyramidal layer in the stratum lucidum corresponding to Mf–CA3 synapses. This staining is lost in GluK2$^{-/-}$ mice. ***C***, Cartoon representing an APP/PS1 mouse model compared with a WT littermate. ***D***, GluK2 staining in the CA3 region of APP/PS1 mice is decreased in comparison to WT. ***E***, Quantification of raw mean pixel intensity in the stratum lucidum region of images as in ***D***. Data were normalized to the mean intensity of the WT condition. ***F***, GluK5 staining in the CA3 region of the APP/PS1 mice is similar to that for WT mice. ***G***, Quantification, as in ***E***, shows no detectable decrease of GluK5. *$p < 0.05$ and ns = non-significant.

Mf-EPSCs (<10%) and can be better analyzed at a stimulation frequency of 3 Hz. We found that KAR-EPSCs were significantly smaller in 6-month-old APP/PS1 mice (Fig. 2*D*,*E*), as clearly indicated by a drop in the ratio between the amplitude of KAR-EPSCs and full Mf-EPSCs (mediated by AMPAR and KARs; 5.4 ± 0.4% to 3.0 ± 3.9%; $n = 13$; *t* test, $p = 0.0005$) between APP/PS1 and WT control mice (Fig. 2*F*). We also observed a striking difference in the decay kinetics of KAR-EPSCs between APP/PS1 and WT control mice (reduction by 24.6% in APP/PS1; Fig. 2*G*). In contrast, synaptic AMPARs and NMDARs are spared at least in basal stimulation conditions, as indicated by similar amplitudes of Mf-CA3 EPSCs at 0.1 Hz (Fig. 2*B*) and of the AMPA/NMDA ratio (Viana da Silva et al., 2019) in APP/PS1 mice compared with control mice. These results indicate that synaptic KARs are selectively altered at Mf–CA3 synapses in this mouse model of AD. Moreover, we found that inward currents evoked by bath application of kainate in CA3 pyramidal neurons were downregulated in APP/PS1 compared with WT controls (348.2 ± 49.8 pA in WT mice vs 227.5 ± 29.1 pA in APP/PS1 mice; Fig. 2*H–J*). Thus, there is likely a selective loss of KARs at Mf–CA3 synaptic sites in APP/PS1 mice, without a potential redistribution of KARs to nonsynaptic sites. This observation is consistent with the knowledge that KARs are not found at nonsynaptic sites in control conditions (Fièvre et al., 2016).

Postsynaptic deletion of presenilin decreases KAR-EPSCs at Mf–CA3 synapses

The APP/PS1 mice used in this study express the APP gene with the Swedish mutations (KM670/671NL) and the presenilin 1 (PSEN1) gene with a deletion of exon 9 (Jankowsky et al., 2004; Garcia-Alloza et al., 2006). These transgenes significantly alter the γ-cleavage of APP, leading to an increase in the production of aggregation-prone amyloid peptides like Aβ42, which, in turn, results in the early formation of amyloid plaques (starting at 6 months). To test whether the impaired synaptic expression of KARs resulted from a more general impairment of PS-mediated function, we compared APP/PS1 mice to a mouse model in which PS is genetically deleted in CA3 pyramidal cells. We targeted the expression of the Cre recombinase (combined with GFP) in the CA3 pyramidal cells of PS1floxed/PS2KO mice *in vivo* (Fig. 3*A–C*). Twenty to 40 d postinfection, we prepared hippocampal slices and recorded Mf-CA3 EPSCs in CA3 pyramidal cells either labeled with GFP (PSdKO cells) or nonlabeled (control cells; Fig. 3*D*). We first evaluated potential changes in the basal synaptic properties. The average amplitude of AMPAR-EPSCs recorded at 0.1 Hz was not different between the two cell types (WT cells, 73 pA; PSdKO, 70 pA; $n = 11$; $p = 0.8572$, *t* test; Fig. 3*E*), indicating that PS does not impact the basal content of synaptic AMPARs or presynaptic release properties (failure rates are similar at 14%; $n = 11$; $p = 0.9450$, *t* test). Unexpectedly, we found a marked decrease in AMPAR-EPSC amplitudes at 3 Hz (WT cells, 367 pA; PsdKO cells, 232 pA; Fig. 3*F*), hence the impairment in frequency facilitation, a characteristic form of short-term synaptic plasticity at Mf–CA3 synapses (Rebola et al., 2017). This impairment in short-term plasticity could be related either to the fact that the Cre recombinase is also expressed in DG cells, hence perturbing short-term plasticity at a presynaptic level (Barthet et al., 2018); or to a transsynaptic consequence of deleting PS from the postsynaptic compartment. We then

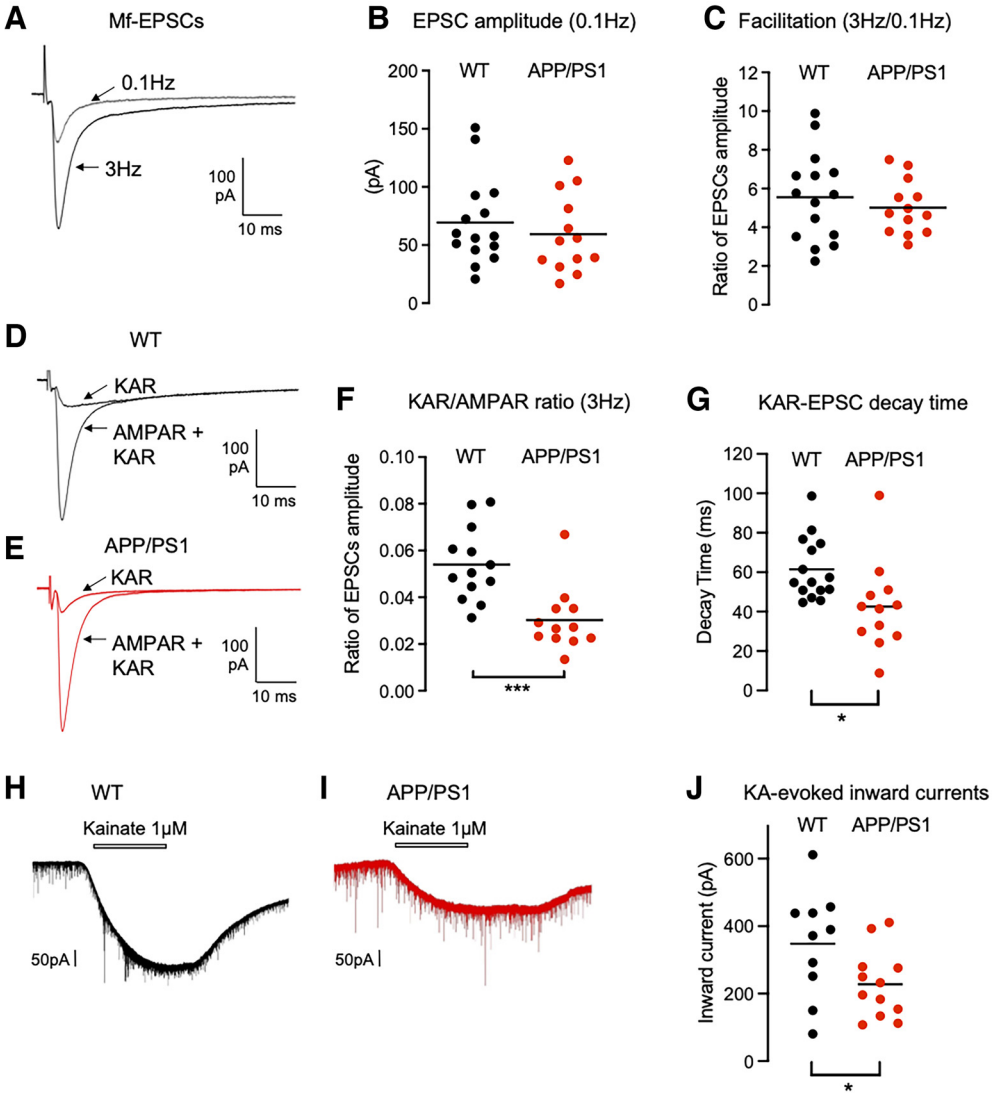

Figure 2. Impaired KAR-mediated synaptic transmission in APP/PS1 mice. ***A***, Representative traces of EPSCs recorded at a stimulation frequency of 0.1 or 3 Hz under conditions in which both AMPAR and KAR currents are active. ***B***, Scatter plots with averages of the EPSC amplitude recorded at 0.1 Hz demonstrate that basal synaptic transmission is not altered in APP/PS1 mice ($n = 15$/genotype). ***C***, Frequency facilitation, represented by the ratio of the amplitude of EPSCs at 3 Hz normalized to the amplitude of EPSCs at 0.1 Hz, is not altered in APP/PS1 mice. ***D***, ***E***, Representative traces of EPSCs recorded at 3 Hz in WT (***D***) or APP/PS1 (***E***) mice under conditions where both AMPAR and KAR currents are active (continuous line) or when KAR currents have been pharmacologically isolated. ***F***, Amplitude of KAR-EPSCs normalized to AMPAR-EPSCs recorded at 3 Hz. The relative amplitude of KAR-EPSCs is significantly lower in APP/PS1 mice. ***G***, Average decay times of KAR-EPSCs are markedly decreased in APP/PS1 mice. ***H***, ***I***, Representative traces of inward currents evoked by bath application of kainate (1 μM) recorded in CA3 pyramidal neurons voltage clamped at −70 mV; the extracellular medium contained bicuculline (10 μM), D-AP5 (50 μM), and tetrodotoxin (500 nM). ***J***, Amplitude of kainate-evoked currents after 2 min bath application in WT and APP/PS1 mice ($n = 10$–12 cells for each condition). *$p < 0.05$, ***$p < 0.001$.

isolated KAR-EPSCs and normalized their amplitude to that of AMPAR-EPSCs to account for changes in glutamate release. We found that the KAR/AMPAR ratio was severely decreased, compared with control CA3 cells (2.5 ± 0.4% vs 0.08 ± 0.3%; $n = 11$; $p = 0.0033$, t test; Fig. 3*G–I*). As in APP/PS1 mice, the reduced amplitude of KAR-EPSCs was accompanied with a marked decrease in their decay kinetics (50.1% of reduction from control; $p < 0.01$, t test; Fig. 3*J*).

We further analyzed GluK2 and GluK5 immunofluorescence labeling in the Cre-infected CA3 subregion of PS1floxed/PS2KO mice, compared with the noninfected contralateral CA3 (Fig. 3*K*, *M*). The efficiency of infection was on the order of 60% of cells infected. We observed a consistent decrease in the staining for GluK2 in the stratum lucidum of Cre-infected CA3 compared with contralateral CA3 (Fig. 3*L*). Quantification of the intensity of fluorescence (see Materials and Methods) showed a marked reduction of GluK2 labeling (but not of GluK5 labeling; Fig. 3*N*), although the efficiency of infection was not maximal. Overall, our data show that presenilin controls the postsynaptic KAR content at Mf–CA3 synapses, and the decay kinetics of synaptic KARs.

A γ-secretase inhibitor decreases the expression of synaptic KARs

Some functions of PS have been reported to not depend on its γ-secretase-related proteolytic activity (Tu et al., 2006; Kallhoff-Munoz et al., 2008). To test whether the impairment of KAR function resulted from the loss of γ-secretase proteolysis of transmembrane proteins, we treated organotypic hippocampal slices, which preserve KAR-EPSCs at Mf–CA3 synapses (Fièvre

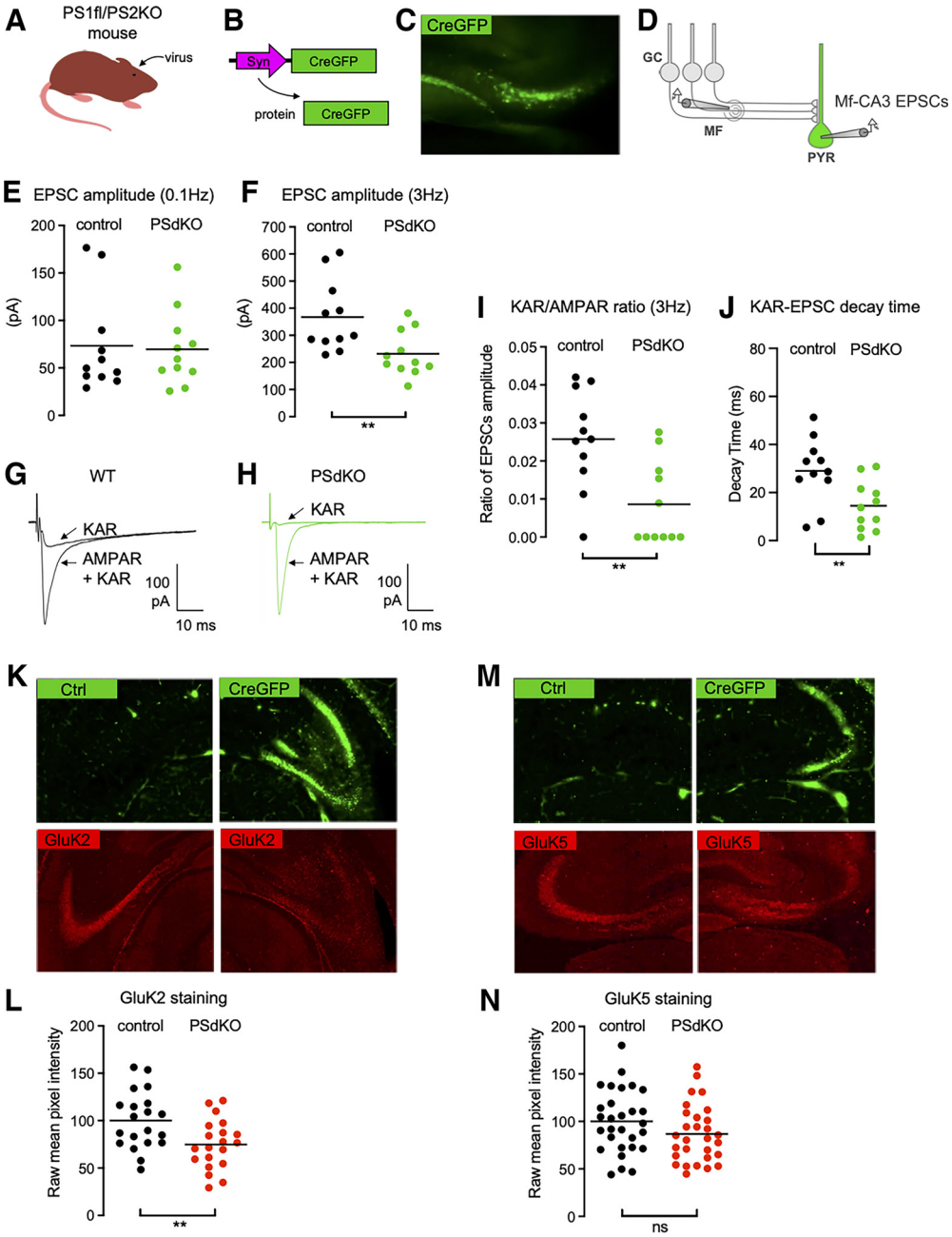

Figure 3. Impaired synaptic expression and function of KARs in the absence of PS. ***A***, Cartoon representing the generation of PSdKO CA3 cells. Cre recombinase-expressing viruses are injected into the CA3 region by stereotaxic surgery. ***B***, Scheme representing the lentiviral vector to express Cre fused to GFP in CA3 pyramidal neurons. ***C***, Representative image of the CA3 region targeted with a virus expressing Cre-GFP. ***D***, Scheme representing the stimulation of Mf that evokes EPSCs recorded in PsdKO CA3 pyramidal neurons (PYR) identified with GFP. ***E***, ***F***, Scatter plots with averages of the EPSC amplitude recorded at 0.1 Hz (***E***) or 3 Hz (***F***) demonstrate that synaptic basal transmission (at 0.1 Hz) is not altered in the postsynaptic PSdKO condition, whereas synaptic transmission is decreased at 3 Hz ($n = 11$/genotype), indicating impaired frequency facilitation. ***G***, ***H***, Representative traces of EPSCs recorded at 3 Hz in WT mice (***G***) or in postsynaptic PSdKO mice (***H***) under conditions where both AMPAR and KAR currents are active or when KAR currents have been pharmacologically isolated. ***I***, Amplitude of KAR-EPSCs normalized to AMPAR-EPSCs recorded at 3 Hz. The relative amplitude of KAR-EPSCs is significantly lower in the postsynaptic PSdKO condition. ***J***, Average decay times of KAR-EPSCs are markedly decreased in PsdKO conditions mice. ***K***, GluK2 staining in the CA3 region of PS1fl/PS2 conditional KO mice targeted (right) or not (left) with a Cre-GFP-expressing virus. The staining is decreased in the postsynaptic PSdKO condition. ***L***, Quantification of raw mean pixel intensity in the stratum lucidum region of images, as in ***J***. Data were normalized to the mean intensity of the WT condition. ***M***, GluK5 staining in the CA3 region of the PSdKO mice is similar to WT mice. ***N***, Quantification as in ***K*** shows no statistically significant decrease of GluK5. $^{**}p < 0.01$. ns = non-significant.

et al., 2016) with a GSI (L685,458 at 10 μM) for at least 4 d (from 10 DIV, after *in vitro* rewiring and synaptogenesis; Fig. 4*A*). We recorded from Mf–CA3 synapses and did not observe any significant change in the amplitude of the AMPAR-EPSCs at 3 Hz (Fig. 4*B*,*C*). When comparing the cell-by-cell ratio of amplitudes of KAR-EPSCs versus AMPAR-EPSCs at 3 Hz, we observed a significant decrease in the KAR/AMPAR ratio in the presence of the GSI (Fig. 4*D*; 10.1 ± 1.4% vs 6.6 ± 0.9%; $n = 13$; $p = 0.046$, *t* test).

Full-length APP interacts with GluK2/GluK5 KARs

The regulation of KAR synaptic expression and function by the proteolytic activity of γ-secretase indicates the involvement of proteolytic substrates of PS in the regulation of KARs at

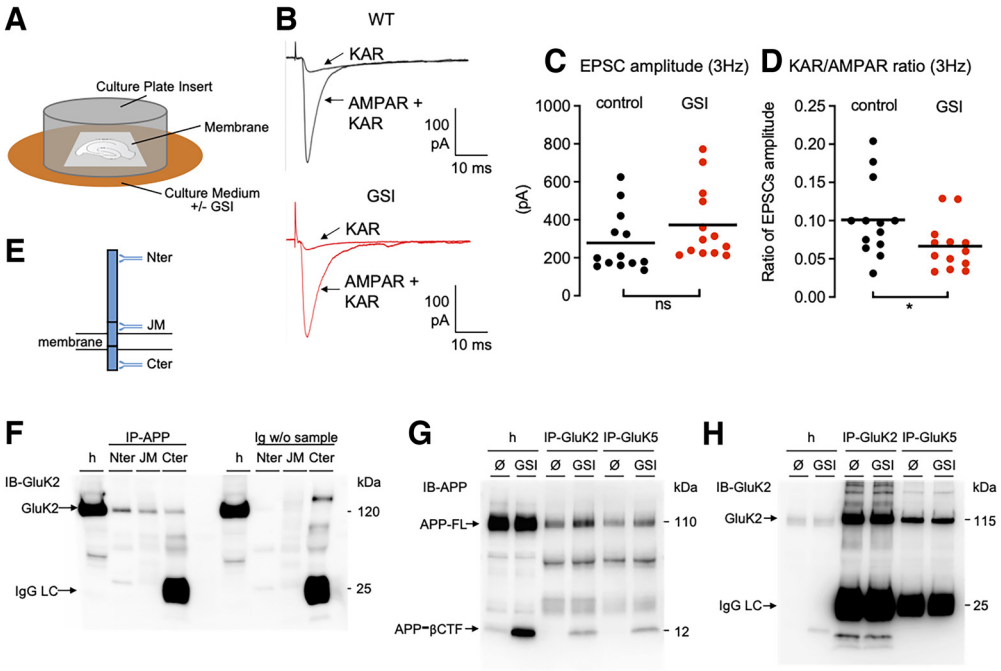

Figure 4. KARs are regulated by γ-secretase proteolytic function and interact with APP. ***A***, Cartoon representing organotypic hippocampal slice cultures and their treatment with a GSI. ***B***, Representative traces of EPSCs recorded at 3 Hz in controls or in the presence of GSI, under conditions where both AMPAR and KAR currents are active or when KAR currents have been pharmacologically isolated. ***C***, Scatter plots with averages of the EPSC amplitude recorded at 3 Hz demonstrate a similar AMPAR-mediated synaptic transmission between control and GSI condition ($n = 13, 14$). ***D***, Amplitude of KAR-EPSCs normalized to AMPAR-EPSCs recorded at 3 Hz. The ratio of KAR-EPSCs versus AMPAR-EPSCs is significantly lower in GSI condition. ***E***, Scheme of APP full-length protein and three antibodies against three different domains (N terminus, juxtamembrane, C terminus). ***F***, Immunoprecipitation of APP, whatever the antibody used and the domain targeted, pulled down GluK2 subunits. The Western-blot band at 120 kDa does not come from the detection of proteins from the beads or from the immunoprecipitating antibodies since the controls without sample (but with beads and immunoprecipitating antibodies) do not contain this band. ***G***, IP of GluK2 or GluK5, pulled down full-length APP (APP-FL) as revealed in the Western blotting of IP eluates. Treatment with γ-secretase inhibitor L685,458 causes the accumulation of APP-CTFs. In this condition, APP-CTFs coimmunoprecipitated with GluK2 or GluK5. ***H***, GluK2 is highly enriched in GluK2-IP eluates. Importantly, GluK5-IP also enriches GluK2 compared with the homogenate (h), indicating strong heterodimerization of GluK2 with GluK5. $^*p < 0.05$; ns = non-significant.

synapses. We have chosen to first investigate a molecular relationship between KARs and APP. Indeed, APP is the main substrate of PS, and its metabolism is particularly altered in the absence of PS [i.e., APP-C-terminal fragments (CTFs) accumulate in cells knocked out by PS or treated with GSI]. Using brain homogenates, we pulled down APP by immunoprecipitation with antibodies against three different domains (N terminus, juxtamembrane, C terminus). GluK2 was coimmunoprecipitated in all three conditions, demonstrating that it likely interacts with the full-length form of APP (Fig. 4*E*,*F*). In cultured hippocampal neurons, we could show that full-length APP was coimmunoprecipitated using antibodies against both GluK2 and GluK5. We could observe that GluK2/GluK5 also interacts with the β-CTF of APP in neuronal cultures treated with GSI, in which this fragment accumulates (Fig. 4*G*). Overall, these data indicate that GluK2/GluK5 interacts with full-length APP, possibly through a domain located in its β-CTF.

Postsynaptic deletion of APP impairs synaptic KARs

Because the level of synaptic KARs is controlled by PS and because APP, a major substrate of PS, interacts with GluK2/GluK5, we next tested whether the reduced synaptic expression of KARs upon deletion of PS was linked to APP. We targeted the expression of the Cre recombinase (combined with GFP) in the CA3 pyramidal cells of APPfloxed/APLP2floxed mice *in vivo*. Twenty to 40 d postinfection, we recorded Mf-CA3 EPSCs in CA3 pyramidal cells in slices, either labeled with GFP (APP/APLP2-dKO cells) or nonlabeled (control cells; Fig. 5*A*–*C*). The amplitude of AMPAR-EPSCs recorded at 0.1 Hz was not different between the two cell types (WT cells, 43.7 ± 6.4 pA; APP/APLP2-KO cells, 55.9 ± 5.6 pA; Fig. 5*D*), indicating that APP (and APLP2) does not have an impact on the basal equipment in synaptic AMPARs or presynaptic release properties (for both groups, similar failure rates at ∼20%; WT cells, $n = 17$; APP/APLP2-KO, $n = 25$; $p = 0.9242$). No change in AMPAR-EPSC amplitudes at 3 Hz (WT cells, 211.6 ± 30.9 pA; vs APP/APLP2-KO cells, 225.2 ± 24.6 pA; $p = 0.7304$) was observed (Fig. 5*E*), hence no change in frequency facilitation (WT cells, 5.28 ± 0.8; vs APP/APLP2-KO cells, 4.06 ± 0.3; $p = 0.1090$). We then isolated KAR-EPSCs at 3 Hz and normalized their amplitude to that of AMPAR-EPSCs. We found that the KAR/AMPAR ratio was severely decreased, compared with control CA3 cells (WT cells, 4.2 ± 1.0%; vs APP/APLP2-KO, 1.3 ± 0.3%; $n = 16$–25; $p = 0.0022$; Fig. 5*F*–*H*). As in APP/PS1 and in PS conditional KO (cKO) CA3 pyramidal cells, the reduced amplitude of KAR-EPSCs was accompanied with a marked decrease in their decay kinetics (reduction by 33.1% from WT cells; $p < 0.01$, *t* test; Fig. 5*I*). These results strongly suggest that the interaction of GluK2/GluK5 KARs with APP stabilizes KARs at Mf–CA3 synapses, and that this process is under the control of the γ-secretase processing of APP by PS. Furthermore, as in the APP/PS1 mice (Viana da Silva et al., 2019), the ratio between synaptic NMDARs and AMPARs measured at +40 vs −70 mV, was not significantly different in APP/APLP2 cKO cells, both at 0.1 Hz ($p = 0.3943$) and at 1 Hz ($p = 0.0966$) stimulation frequency (Fig. 5*J*–*L*). Hence, synaptic KARs appear to be selectively impacted in APP/APLP2 cKO CA3 pyramidal cells, in contrast to synaptic AMPA and NMDA receptors, which appear to be unaffected.

Discussion

Alzheimer's disease pathology involves synaptic dysfunction in its early stages (Sheng et al., 2012). Both PS and APP, the two genes involved in the familial early-onset form of the disease, have been identified to play significant role in synaptic transmission (Shen, 2014; Müller et al., 2017). Understanding the regulation of synaptic receptors by PS and APP is fundamental because alteration of the physiological function of PS or APP could contribute to AD pathology (Shen, 2014). Synaptic function and plasticity have been extensively studied in mouse models in the context of AD (Marchetti and Marie, 2011; Sheng et al., 2012). Within these studies, the synaptic function and trafficking of AMPA and NMDA receptors were shown to be compromised in the presence of pathologic concentrations of Aβ or in mouse models of AD (Sheng et al., 2012). In contrast, there has yet been no report, to our knowledge, on the link between KARs, the third family of ionotropic glutamate receptors, and AD, in either experimental models or in human patients.

Here we first found that immunohistological labeling of GluK2 was markedly decreased in the stratum lucidum of APP/PS1 mice, at 6 months of age. The stratum lucidum corresponds to the site of synaptic contacts of mossy fibers onto the proximal dendrites of CA3 pyramidal cells. KARs comprising the GluK2 subunit are known to be expressed both at the presynaptic and the postsynaptic sites in Mf–CA3 synapses (Mulle et al., 1998; Contractor et al., 2001). At the postsynaptic site in CA3 PCs, GluK2-containing KARs are highly compartmentalized at Mf–CA3 synapses (Fièvre et al., 2016). We then found that the amplitude of KAR-EPSCs was markedly decreased in APP/PS1 mice; in contrast, we found no change in presynaptic short-term plasticity, which is known to depend on presynaptic GluK2-containing KARs (Contractor et al., 2001). Hence, the loss of GluK2 immunolabeling can be attributed to a reduced expression of KARs at the postsynaptic site. In contrast to GluK2, the immunolabeling of GluK5 did not significantly decrease in the APP/PS1 condition. This is at odds with the view that GluK5 labeling is suppressed in GluK2 KO mice (Christensen et al., 2004; Ruiz et al., 2005). A possible explanation for the lack of apparent change in GluK5 may be that it is a limiting subunit within the heterodimer. Indeed, unlike GluK2 KO mice, GluK2 is only reduced in APP/PS1 mice and the remaining pool

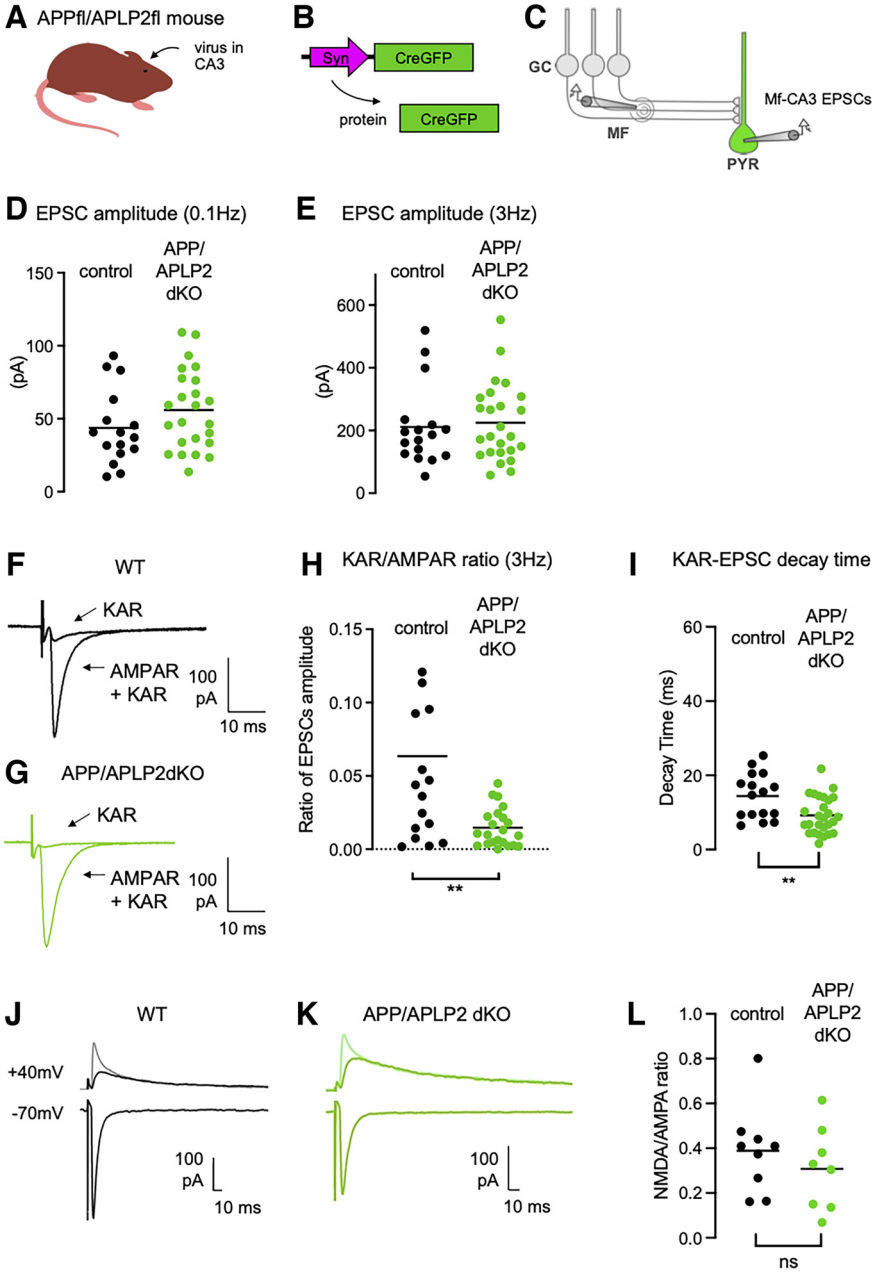

Figure 5. Impaired synaptic expression and function of KARs in the absence of APP. ***A***, Cartoon representing the APP/APLP2 floxed mouse model. Cre recombinase-expressing viruses are injected into the CA3 region by stereotaxic surgery. ***B***, Scheme representing the viral vector to express Cre fused to GFP in CA3 pyramidal neurons. ***C***, Scheme representing the stimulation of Mf that evokes EPSCs recorded in CA3 pyramidal neurons (PYR) genetically manipulated (Cre-mediated APP/APLP2 genes deletion) and identified with GFP. ***D***, ***E***, Scatter plots with averages of the EPSC amplitude recorded at 0.1 Hz (***D***) or 3 Hz (***E***) demonstrate that basal synaptic transmission (at 0.1 Hz) and frequency facilitation is not altered in postsynaptic APP/APLP2 KO condition. ***F***, ***G***, Representative traces of EPSCs recorded at 3 Hz in WT mice (***F***) or in postsynaptic APP/APLP2 KO mice (***G***) under conditions where both AMPAR and KAR currents are active or when KAR currents have been pharmacologically isolated. ***H***, Amplitude of KAR-EPSCs normalized to AMPAR-EPSCs recorded at 3 Hz. The relative amplitude of KAR-EPSCs is significantly lower in postsynaptic APP/APLP2 KO condition. ***I***, Average decay times of KAR-EPSCs are markedly decreased in APP/APLP2 KO conditions. $^{**}p < 0.01$. ***J***, ***K***, Representative traces of Mf-EPSCs recorded at negative (−70 mV) and positive holding potentials (+40 mV), without (lighter color trace) and with NBQX (20 μM) to isolate NMDAR-mediated currents. Bicuculline (10 μM) was present throughout all the recordings. ***L***, Mean values of NMDAR/AMPAR ratios at a frequency of stimulation of 0.1 Hz, calculated from the peak amplitude of AMPAR-EPSCs recorded at −70 mV and the peak amplitude of NMDAR-EPSCs at +40 mV (without NBQX). The ratio is not altered in APP/APLP2 dKO conditions ($n = 8–9$ cells, $p = 0.3943$).

may be sufficient to maintain GluK5, although not expressed at the plasma membrane. Importantly, we did not find any evidence for a change in the amplitude of AMPAR-mediated or NMDAR-mediated EPSCs in basal stimulating conditions in 6-month-old APP/PS1 mice (Viana da Silva et al., 2019), indicating a selective downregulation of postsynaptic KARs.

Because APP/PS1 mice overexpress a mutant form of PS (PS1Δ9), we tested whether the synaptic phenotype observed could be mimicked by deleting PS in postsynaptic CA3 PCs. We found that the amplitude of KAR-EPSCs was similarly decreased in CA3 PCs, in parallel with a decreased immunolabeling of GluK2 in the stratum lucidum. Interestingly, a similar phenotype was observed in organotypic hippocampal cultures treated with γ-secretase inhibitors. These experiments strongly suggested that the mechanisms underlying the control of synaptic KARs depends on PS and on its γ-secretase proteolytic activity.

The γ-secretase complex promotes the cleavage of a large number of cell surface proteins found at synaptic contacts, such as transsynaptic adhesion molecules (Barthet et al., 2011). For example, N-cadherin is well known to undergo sequential processing, first by ADAM-10 at the juxtamembrane region, leading to a membrane-tethered C-terminal fragment, CTF1 (Marambaud et al., 2003), and then by PS at the transmembrane segment releasing the CTF2 peptide into the cytoplasm (Marambaud et al., 2003; Malinverno et al., 2010). We have demonstrated that N-cadherin is involved in the synaptic stabilization of KARs (Fièvre et al., 2016). We may thus hypothesize that the genetic or pharmacological invalidation of PS disrupts transsynaptic N-cadherin interaction and impacts synaptic KARs at Mf–CA3 synapses. However, APP, a major substrate of PS is also known to form *trans* dimers at the neuromuscular junction and central synapses, enabling them to function as synaptic adhesion molecules (Müller et al., 2017). We show here that both GluK2 and GluK5, which form native heterodimers (Wenthold et al., 1994), interact with both the C terminus and N terminus of APP; hence the full-length protein. The genetic removal of APP (and APLP2) from postsynaptic CA3 pyramidal cells leads to a marked reduction of synaptic KAR-EPSCs. These experiments suggest that APP stabilizes GluK2/GluK5 containing KARs at Mf–CA3 synapses, possibly through its role as a transsynaptic protein. This process appears to be under the control of the γ-secretase activity of PS. The disruption of γ-secretase activity may lead to an imbalance of the cleavage by-products of APP (and possibly N-cadherin), with an increased level of the β-CTF of APP, which is shown to be immunoprecipitated by GluK2 and GluK5 antibodies. KARs bound to the β-CTF of APP may escape then from transsynaptic APP, hence from synaptic sites.

Importantly, in all genetic conditions tested (APP/PS1, PS cKO and APP/APLP2 cKO), the reduced amplitude of KAR-EPSCs at Mf–CA3 synapses was accompanied with a marked decrease in their decay kinetics. These features directly phenocopy the Neto1 KO phenotype (Straub et al., 2011; Tang et al., 2011), allowing us to propose the following hypothetical mechanism (Fig. 6). Neto1, as an auxiliary subunit, directly interacts with synaptic KARs at Mf–CA3 synapses (Copits and Swanson, 2012). We hypothesize that Neto1 may serve as a link for the interaction of KARs with APP, which acts as a transmembrane synaptic adhesion protein similar to what was shown at other synapses (Müller et al., 2017). APP thus may act as a synaptic

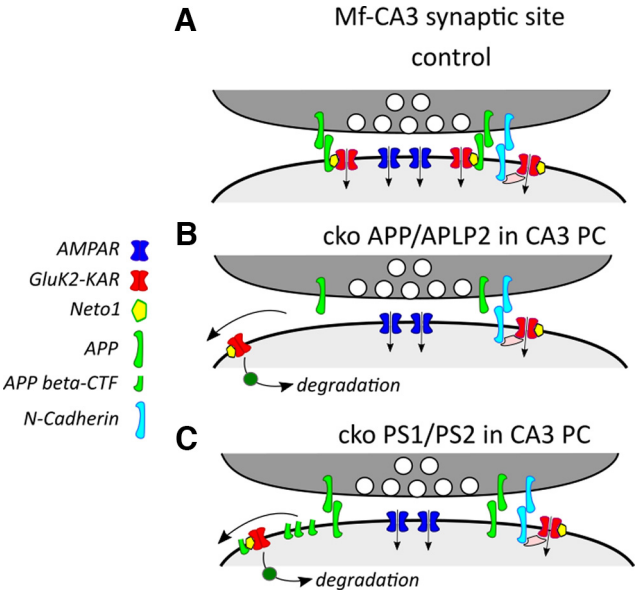

Figure 6. Hypothetical mechanism for the role of APP and PS in the stabilization of KARs at Mf–CA3 synapses. ***A***, Representative scheme of a synaptic site with Mf–CA3 synapses in control conditions. APP is expressed at presynaptic and postsynaptic sites and acts as a transmembrane adhesion protein. We hypothesize that APP interacts with Neto1, an auxiliary subunit of KARs present at Mf–CA3 synapses, therefore providing a mechanism for anchoring KARs at these synaptic sites. KARs are likely to be recruited and stabilized by additional mechanisms (including N-cadherins or C1ql2). ***B***, In the absence of APP from postsynaptic CA3 pyramidal cells, KARs may loose its anchor to transsynaptic adhesion molecules and be destabilized from synapses. Extrasynaptic KARs are sent to degradation pathways. ***C***, In the absence of PS from postsynaptic CA3 pyramidal cells, there is an accumulation of the APP βCTF, which competes for the interaction of APP with the Neto1/KAR complex, which in turn destabilizes KARs from synapses.

stabilizer of KARs at Mf–CA3 synapses through interaction with Neto1, possibly through a domain located in its β-CTF. In the absence of APP, the KAR/Neto1 complex is destabilized, removed from synaptic sites, and sent to degradation pathways. In the absence of PS, the β-CTFs accumulate in synaptic sites. The complex formed by KARs, Neto1, and APP β-CTF may then be destabilized from synaptic sites and sent to degradation pathways. Multiple mechanisms may recruit and stabilize KARs at Mf–CA3 synapses, including N-cadherins (Fièvre et al., 2016) and C1ql2/3 proteins (Matsuda et al., 2016). Hence, the absence of APP (or Neto1) does not lead to full suppression of synaptic KARs. This hypothetical scheme should be directly tested in the future using Neto1-selective appropriate tools when they become available.

Whatever the mechanism, our results provide strong evidence for a physiological role of APP and its metabolism by PS in regulating the recruitment and/or the stabilization of synaptic KARs. What would be the consequence of a loss of synaptic KARs at Mf–CA3 synapses in the context of AD? Because of their slow decay kinetics, EPSCs mediated by KARs are important for the integration of synaptic signals, particularly during bursts of incoming inputs (Sachidhanandam et al., 2009; Pinheiro et al., 2013). This implies that in conditions of reduced PS activity, the transfer of spikes between the DG and CA3 will be impaired, in response to the typical bursting activity of the presynaptic DG cells. It is thought that DG projections to CA3 support memory through pattern separation and may be important to the initiation of oscillations, such as sharp-wave ripples, involved in working memory (Sasaki et al., 2018). Overall, the destabilization of synaptic KARs in the CA3 may participate in the difficulties in forming new memories in AD patients. Aberrant synaptic KARs

expressed at aberrant recurrent fibers from DG cells (Epsztein et al., 2005) are critically involved in the generation of the chronic epileptic discharges in animal models of TLE (Peret et al., 2014). Here, we observe a reduction of synaptic KARs, which would rather limit the propagation of neuronal activity within the hippocampus. Hence, the PS-mediated control of synaptic KARs may not play any role in neuronal hyperactivity and in the epileptic propensity of AD. However, our study clearly indicates that KARs should be better taken into consideration whenever addressing synaptic dysfunction in the context of AD.

References

Barthet G, Shioi J, Shao Z, Ren Y, Georgakopoulos A, Robakis NK (2011) Inhibitors of -secretase stabilize the complex and differentially affect processing of amyloid precursor protein and other substrates. FASEB J 25:2937–2946.

Barthet G, Georgakopoulos A, Robakis NK (2012) Cellular mechanisms of γ-secretase substrate selection, processing and toxicity. Prog Neurobiol 98:166–175.

Barthet G, Jordà-Siquier T, Rumi-Masante J, Bernadou F, Müller U, Mulle C (2018) Presenilin-mediated cleavage of APP regulates synaptotagmin-7 and presynaptic plasticity. Nat Commun 9:4780.

Carta M, Lanore F, Rebola N, Szabo Z, Da Silva SV, Lourenço J, Verraes A, Nadler A, Schultz C, Blanchet C, Mulle C (2014a) Membrane lipids tune synaptic transmission by direct modulation of presynaptic potassium channels. Neuron 81:787–799.

Carta M, Fièvre S, Gorlewicz A, Mulle C (2014b) Kainate receptors in the hippocampus. Eur J Neurosci 39:1835–1844.

Castillo PE, Malenka RC, Nicoll RA (1997) Kainate receptors mediate a slow postsynaptic current in hippocampal CA3 neurons. Nature 388:182–186.

Christensen JK, Paternain AV, Selak S, Ahring PK, Lerma J (2004) A mosaic of functional kainate receptors in hippocampal interneurons. J Neurosci 24:8986–8993.

Contractor A, Swanson G, Heinemann SF (2001) Kainate receptors are involved in short- and long-term plasticity at mossy fiber synapses in the hippocampus. Neuron 29:209–216.

Contractor A, Mulle C, Swanson GT (2011) Kainate receptors coming of age: milestones of two decades of research. Trends Neurosci 34:154–163.

Copits BA, Swanson GT (2012) Dancing partners at the synapse: auxiliary subunits that shape kainate receptor function. Nat Rev Neurosci 13:675–686.

Crépel V, Mulle C (2015) Physiopathology of kainate receptors in epilepsy. Curr Opin Pharmacol 20:83–88.

De Strooper B, Saftig P, Craessaerts K, Vanderstichele H, Guhde G, Annaert W, Von Figura K, Van Leuven F (1998) Deficiency of presenilin-1 inhibits the normal cleavage of amyloid precursor protein. Nature 391:387–390.

Epsztein J, Represa A, Jorquera I, Ben-Ari Y, Crépel V (2005) Recurrent mossy fibers establish aberrant kainate receptor-operated synapses on granule cells from epileptic rats. J Neurosci 25:8229–8239.

Fièvre S, Carta M, Chamma I, Labrousse V, Thoumine O, Mulle C (2016) Molecular determinants for the strictly compartmentalized expression of kainate receptors in CA3 pyramidal cells. Nat Commun 7:12738.

Garcia-Alloza M, Robbins EM, Zhang-Nunes SX, Purcell SM, Betensky RA, Raju S, Prada C, Greenberg SM, Bacskai BJ, Frosch MP (2006) Characterization of amyloid deposition in the APPswe/PS1dE9 mouse model of Alzheimer disease. Neurobiol Dis 24:516–524.

Jankowsky JL, Fadale DJ, Anderson J, Xu GM, Gonzales V, Jenkins NA, Copeland NG, Lee MK, Younkin LH, Wagner SL, Younkin SG, Borchelt DR (2004) Mutant presenilins specifically elevate the levels of the 42 residue beta-amyloid peptide in vivo: evidence for augmentation of a 42-specific gamma secretase. Hum Mol Genet 13:159–170.

Kallhoff-Munoz V, Hu L, Chen X, Pautler RG, Zheng H (2008) Genetic dissection of gamma-secretase-dependent and -independent functions of presenilin in regulating neuronal cell cycle and cell death. J Neurosci 28:11421–11431.

Lerma J, Marques JM (2013) Kainate receptors in health and disease. Neuron 80:292–311.

Malinverno M, Carta M, Epis R, Marcello E, Verpelli C, Cattabeni F, Sala C, Mulle C, Di Luca M, Gardoni F (2010) Synaptic localization and activity of ADAM10 regulate excitatory synapses through N-cadherin cleavage. 30. J Neurosci 30:16343–16355.

Marambaud P, Wen PH, Dutt A, Shioi J, Takashima A, Siman R, Robakis NK (2003) A CBP binding transcriptional repressor produced by the PS1/ϵ-cleavage of N-cadherin is inhibited by PS1 FAD mutations. Cell 114:635–645.

Marchal C, Mulle C (2004) Postnatal maturation of mossy fibre excitatory transmission in mouse CA3 pyramidal cells: a potential role for kainate receptors. J Physiol 561:27–37.

Marchetti C, Marie H (2011) Hippocampal synaptic plasticity in Alzheimer's disease: what have we learned so far from transgenic models? Rev Neurosci 22:373–402.

Matsuda K, Budisantoso T, Mitakidis N, Sugaya Y, Miura E, Kakegawa W, Yamasaki M, Konno K, Uchigashima M, Abe M, Watanabe I, Kano M, Watanabe M, Sakimura K, Aricescu AR, Yuzaki M (2016) Transsynaptic modulation of kainate receptor functions by C1q-like proteins. Neuron 90:752–767.

Mulle C, Crépel V (2021) Regulation and dysregulation of neuronal circuits by KARs. Neuropharmacology 197:108699.

Mulle C, Sailer A, Pérez-Otaño I, Dickinson-Anson H, Castillo PE, Bureau I, Maron C, Gage FH, Mann JR, Bettler B, Heinemann SF (1998) Altered synaptic physiology and reduced susceptibility to kainate-induced seizures in GluR6-deficient mice. Nature 392:601–605.

Müller UC, Deller T, Korte M (2017) Not just amyloid: physiological functions of the amyloid precursor protein family. Nat Rev Neurosci 18:281–298.

Peret A, Christie LA, Ouedraogo DW, Gorlewicz A, Epsztein J, Mulle C, Crépel V (2014) Contribution of aberrant GluK2-containing kainate receptors to chronic seizures in temporal lobe epilepsy. Cell Rep 8:347–354.

Pinheiro PS, Lanore F, Veran J, Artinian J, Blanchet C, Crépel V, Perrais D, Mulle C (2013) Selective block of postsynaptic kainate receptors reveals their function at hippocampal mossy fiber synapses. Cereb Cortex 23:323–331.

Rebola N, Carta M, Mulle C (2017) Operation and plasticity of hippocampal CA3 circuits: implications for memory encoding. Nat Rev Neurosci 18: 208–220.

Ruiz A, Sachidhanandam S, Utvik JK, Coussen F, Mulle C (2005) Distinct subunits in heteromeric kainate receptors mediate ionotropic and metabotropic function at hippocampal mossy fiber synapses. J Neurosci 25:11710–11718.

Sachidhanandam S, Blanchet C, Jeantet Y, Cho YH, Mulle C (2009) Kainate receptors act as conditional amplifiers of spike transmission at hippocampal mossy fiber synapses. J Neurosci 29:5000–5008.

Sasaki T, Piatti VC, Hwaun E, Ahmadi S, Lisman JE, Leutgeb S, Leutgeb JK (2018) Dentate network activity is necessary for spatial working memory by supporting CA3 sharp-wave ripple generation and prospective firing of CA3 neurons. Nat Neurosci 21:258–269.

Shen J (2014) Function and dysfunction of presenilin. Neurodegener Dis 13:61–63.

Sheng M, Sabatini BL, Südhof TC (2012) Synapses and Alzheimer's disease. Cold Spring Harbor Perspect Biol 4:a005777.

Sherrington R, Rogaev EI, Liang Y, Rogaeva EA, Levesque G, Ikeda M, Chi H, Lin C, Li G, Holman K (1995) Cloning of a gene bearing missense mutations in early-onset familial Alzheimer's disease. Nature 375:754–760.

Straub C, Hunt DL, Yamasaki M, Kim KS, Watanabe M, Castillo PE, Tomita S (2011) Distinct functions of kainate receptors in the brain are determined by the auxiliary subunit Neto1. Nat Neurosci 14:866–873.

Tang M, Pelkey KA, Ng D, Ivakine E, McBain CJ, Salter MW, McInnes RR (2011) Neto1 is an auxiliary subunit of native synaptic kainate receptors. J Neurosci 31:10009–10018.

Tu H, Nelson O, Bezprozvanny A, Wang Z, Lee SF, Hao YH, Serneels L, De Strooper B, Yu G, Bezprozvanny I (2006) Presenilins form ER Ca^{2+} leak channels, a function disrupted by familial Alzheimer's disease-linked mutations. Cell 126:981–993.

Viana da Silva S, Zhang P, Haberl MG, Labrousse V, Grosjean N, Blanchet C, Frick A, Mulle C (2019) Hippocampal mossy fibers synapses in CA3 pyramidal cells are altered at an early stage in a mouse model of Alzheimer's disease. J Neurosci 39:4193–4205.

Vossel KA, Tartaglia MC, Nygaard HB, Zeman AZ, Miller BL (2017) Epileptic activity in Alzheimer's disease: causes and clinical relevance. Lancet Neurol 16:311–322.

Wenthold RJ, Trumpy VA, Zhu WS, Petralia RS (1994) Biochemical and assembly properties of GluR6 and KA2, two members of the kainate receptor family, determined with subunit-specific antibodies. J Biol Chem 269:1332–1339.